

Accepted Manuscript

Synthesis and microstructural properties of zinc oxide nanoparticles prepared by selective leaching of zinc from spent alkaline batteries using ammoniacal ammonium carbonate

Félix A. López, Teresa Cebriano, Irene García-Díaz, Paloma Fernández, Olga Rodríguez, Ana López Fernández

PII: S0959-6526(17)30236-6

DOI: [10.1016/j.jclepro.2017.02.031](https://doi.org/10.1016/j.jclepro.2017.02.031)

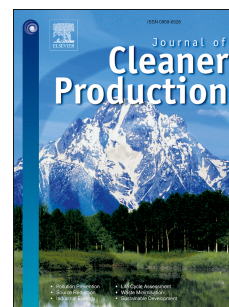
Reference: JCLP 8957

To appear in: *Journal of Cleaner Production*

Received Date: 3 August 2016

Revised Date: 1 February 2017

Accepted Date: 3 February 2017



Please cite this article as: López FA, Cebriano T, García-Díaz I, Fernández P, Rodríguez O, Fernández AL, Synthesis and microstructural properties of zinc oxide nanoparticles prepared by selective leaching of zinc from spent alkaline batteries using ammoniacal ammonium carbonate, *Journal of Cleaner Production* (2017), doi: 10.1016/j.jclepro.2017.02.031.

This is a PDF file of an unedited manuscript that has been accepted for publication. As a service to our customers we are providing this early version of the manuscript. The manuscript will undergo copyediting, typesetting, and review of the resulting proof before it is published in its final form. Please note that during the production process errors may be discovered which could affect the content, and all legal disclaimers that apply to the journal pertain.

Synthesis of ZnO from spent batteries

Leaching

Black mass + $\text{NH}_3/(\text{NH}_4)_2(\text{CO}_3)$

Zincite (ZnO), Hetaerolite (ZnMn_2O_4), Silvite (KCl), Graphite, Ca_5Mn_8

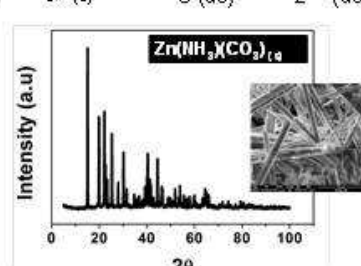
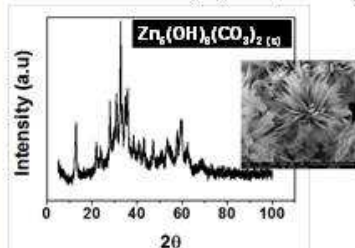
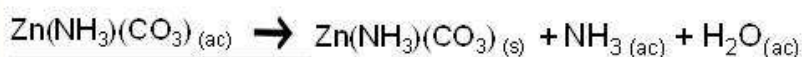
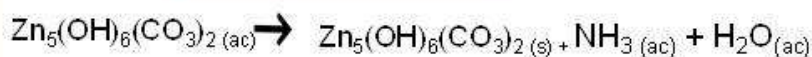
$\text{Zn}_5(\text{OH})_6(\text{CO}_3)_2$ (ac)

0.1 mol/L NH_3
1.72 mol/L $(\text{NH}_4)_2(\text{CO}_3)$

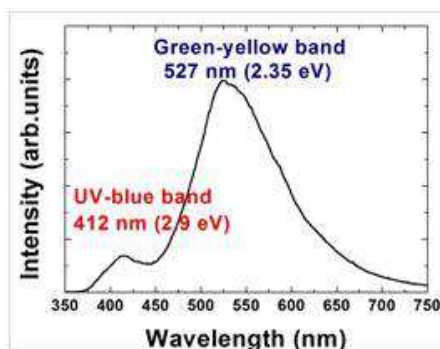
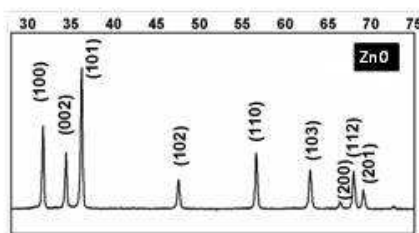
$\text{Zn}(\text{NH}_3)(\text{CO}_3)$ (ac)

0.5 to 1 mol/L NH_3
1.72 mol/L $(\text{NH}_4)_2(\text{CO}_3)$

Evaporation Rotavapor/34 bars/56°C



Calcination 800°C/5 h



Synthesis and Microstructural Properties of Zinc Oxide Nanoparticles Prepared by Selective Leaching of Zinc from Spent Alkaline Batteries using Ammoniacal Ammonium Carbonate

Félix A. López^{1,c}, Teresa Cebriano^{1,2}, Irene García-Díaz¹, Paloma Fernández²,
Olga Rodríguez¹, Ana López Fernández¹

¹ Centro Nacional de Investigaciones Metalúrgicas (CENIM. CSIC), Avda. Gregorio del Amo 8, 28040 Madrid, Spain

²Departamento de Física de Materiales, Facultad de Ciencias Físicas, Universidad Complutense de Madrid (UCM), Ciudad Universitaria, Plaza Ciencias 1, 28040 Madrid, Spain

^c Corresponding author: f.lopez@csic.es

Abstract

Two different precursors of zinc oxide were prepared via the ammoniacal ammonium carbonate leaching of the black mass obtained during the recycling of alkaline batteries. For a concentration of 0.1 mol/L of ammonium in the leaching solution, zinc basic carbonate, was obtained, while for higher ammonium concentrations (0.5 and 1 mol/L), zinc ammonium carbonate was the final product. These precursors were characterised by X-ray diffraction (XRD), Fourier transform infrared spectroscopy (FTIR), Thermogravimetric analysis (TGA/DTG) and Scanning electron microscopy (SEM), and calcined to obtain ZnO. Raman spectroscopy, X-ray diffraction and Transmission electron microscopy (TEM) analysis of the resulting zinc oxide samples indicated a wurtzite hexagonal lattice with *a* parameter values ranging from 3.23 Å to 3.30 Å, and *c* parameter values from 5.18 Å to 5.21 Å (values close to typical). The room temperature photoluminescence spectra of the zinc oxide samples showed two main bands: a high energy UV-blue band centred at either 412 or 382 nm (depending on the NH₃ concentration of the leaching solution used), and a green band centred at 527 nm. These emission bands are comparable to those reported for pure zinc oxide.

Keywords: Spent batteries; zinc oxide; basic zinc carbonate; ammonium zinc carbonate; lixiviation; photoluminescence

1. Introduction

ZnO is one of the most widely studied semiconductors due to its excellent properties for many technological applications. ZnO has attracted much attention as a component of ultraviolet and optoelectronic sensors (Chou et al., 2006), UV lasers (Tang et al., 1998), light emitting diodes (Tsukazaki et al., 2004) and solar cells (Keis et al., 2000), etc., a consequence of its high refractive index and large exciton binding energy (60 meV) at room temperature. ZnO crystallites can be obtained by different chemical and physical synthesis methods involving nanowires, nanobelts or nanorods. Other, more complex ZnO morphologies can be produced that expand its application range (Djurišić et al., 2010).

Several synthesis routes have been developed in order to manufacture or extract pure ZnO, mainly involving synthetic materials as precursor materials (Kołodziejczak-Radzimska and Jesionowski, 2014). One widely used method is the thermal decomposition of different zinc compounds and salts. For example, Audebrand et al., 1998 obtain zinc oxide powders by thermal decomposition of four different precursors (hydroxide nitrate, oxalate, hydroxide carbonate, and acetate); Baskoutas et al., 2007 by thermal decomposition of zinc alginate gels and finally, Khalil et al., 2014, by thermal decomposition of a binuclear zinc (II) curcumin complex.

The most common precursors used in thermal decomposition for obtaining ZnO are the basic zinc carbonate forms $\text{Zn}_5(\text{OH})_6(\text{CO}_3)_2$, $\text{Zn}_4\text{CO}_3(\text{OH})_6 \cdot \text{H}_2\text{O}$ and $\text{Zn}_3\text{CO}_3(\text{OH})_4 \cdot 2\text{H}_2\text{O}$. The $\text{Zn}_5(\text{OH})_6(\text{CO}_3)_2$ is of particular interest given its low decomposition temperature (Tsukazaki et al., 2004). Basic zinc carbonates can be synthesized from zinc acetate dehydrate ($\text{Zn}(\text{CH}_3\text{COOH})_2 \cdot 2\text{H}_2\text{O}$) and urea (NH_2CONH_2) via the sol-gel method (Wahab et al., 2008), by the dissolving of $\text{Zn}(\text{NO}_3)_2 \cdot 6\text{H}_2\text{O}$ and urea in milli-Q water (Bitenc et al., 2008), and from ZnSO_4 solution using $(\text{NH}_4)_2\text{CO}_3$ as a precipitating agent followed by thermal treatment (Li et al., 2005), among others.

On the other hand alkaline batteries (which account for some 85% of all those manufactured (Deep et al., 2011)) have four main components: MnO_2 (the positive

electrode), Zn (the negative electrode), electrolytes (KOH or $\text{ZnCl}_2 + \text{NH}_4\text{Cl}$), and steel (the battery casing). Together, these make up some 93% of the average battery. The collection of spent portable primary and rechargeable batteries in Europe is mandated by Directive 2013/56/EU (European Parliament and the Council, 2013), which required Member States to achieve a collection rate of 25% by 2012 and 45% by 2016. Around 214,000 tonnes of portable batteries (around 10.2 billion batteries) entered the market of the EEA+Switzerland in 2014, and around 85,000 tonnes of spent batteries were collected (European Portable Battery Association, 2015).

A number of pyro- and hydrometallurgical processes have been developed for the treatment of these batteries which allow recovering the main components of these, Zn and Mn. Both types of processes require the grinding and milling of the batteries, followed by the magnetic separation of all their steel components plus the removal of all their plastic and paper parts, to obtain a product known as "black mass". i.e., a black mixture of carbon, ZnO, Zn/Mn oxides, and the battery's electrolytes.

Pyrometallurgical treatment involves the recovery of Zn from this black mass via the Waelz process (Serbent et al., 1980) of carbothermic reduction in a rotary furnace. There are, however, several hydrometallurgical methods for recovering the Zn from alkaline batteries. One of these, leaching with H_2SO_4 , allows some 95% recovery of the Zn, but it also simultaneously recovers some 45% of the Mn (Salgado, 2003); the leachates produced therefore have to be treated to separate these metals. Although most of the iron in batteries is removed during the magnetic separation step, its elimination is not complete. Hence, leaching the black mass of batteries with acid, has the drawback that the leachate is contaminated by iron. To overcome this problem, leaching with NaOH (Senanayake et al., 2010), and ammoniacal- $(\text{NH}_4)_2\text{CO}_3$ solutions have been studied. Zn forms stable complexes in the Zn- CO_2 - NH_3 system, allowing the final recovery of Zn in the form of ZnO via ZnCO_3 intermediates (Buzatu et al., 2013). Leaching with ammoniacal NH_4Cl solution has also been studied; Zn forms stable complexes in the Zn-Cl- NH_3 system (Nogueira and Margarido, 2015).

The present work explores the production of ZnO via the thermal decomposition of $\text{Zn}_5(\text{OH})_6(\text{CO}_3)_2$ and $\text{Zn}(\text{NH}_3)(\text{CO}_3)$ obtained from the ammoniacal- $(\text{NH}_4)_2\text{CO}_3$

leaching of the black mass extracted from alkaline batteries. The ZnO recovered was characterised, and its photoluminescent behaviour at room temperature in the visible and infrared ranges examined.

2. Experimental

2.1. Black mass starting material: characterisation

Black mass starting material from the recycling of Zn-C and alkaline batteries was obtained from Envirobat España S.L. (Guadalajara, Spain). Collected batteries were ground in a mill under an N₂ atmosphere. The steel components were then magnetically separated, and the plastic and paper components removed. The resulting black mass had a grain size of <0.83 mm. The chemical composition of the black mass was determined by X-ray fluorescence using a PANalytical Axios wavelength dispersive spectrometer (4 kW). The mineralogical composition of the black mass was determined by X-ray diffraction (XRD) using a Siemens D5000 diffractometer equipped with a Cu anode (Cu K α radiation) and a LiF monochromator.

2.2. Production of ZnO

ZnO was produced from the black mass in three steps: (i) leaching of the black mass with ammoniacal (NH₄)₂CO₃; (ii) evaporation of the leachate under vacuum, and iii) calcination of the post-evaporation product.

- (i) *Leaching*: The black mass was leached with 1.72 mol/L (NH₄)₂CO₃ (final black mass pulp concentration 100 g/L) at room temperature for 60 min, agitated at 1800 rpm. The concentration of NH₃ added to the leaching solution varied from 0.1 to 1 mol/L. The suspension obtained was filtered under vacuum and the resulting solution (leachate) kept for further processing. An aliquot of the leachate was used for the determination of its Zn and Cu content by atomic absorption spectroscopy.
- (ii) *Evaporation*: representative samples (0.5 L) of the leachate obtained with each leaching solution (i.e., with the different NH₃ concentrations) were evaporated in a Buchi R-100 Rotavapor under a pressure of 34 bars. The resulting solid

(termed 'precursor') was dried in an oven at 80° C for 6 h. A sample of each of the precursors obtained was characterised as described below.

- (iii) *Calcination*: The different precursors were calcined at 800° C for 5 h in a Heraus Model 10003 furnace to obtain ZnO.

2.3. Structural analysis of the precursors and the ZnO obtained from them

All precursor and ZnO samples were characterized by scanning field emission electron microscopy (SFSEM) using a HITACHI S-4800 instrument, and by XRD using a Siemens D-500 X-ray diffractometer.

The precursors were also subjected to Fourier-transformed infrared spectroscopy (FTIR) using a Varian 670 FTIR spectrometer (spectral range 4000-400 cm^{-1} , spectral resolution of 4 cm^{-1}) in transmittance mode. This analysis was performed using a pellet (made following the KBr pellet technique [precursor = 1 wt.%]) of each precursor produced. In addition, the precursors were subjected to thermogravimetric decomposition analysis, performed using 12 mg samples in a SETARAM Sensys Evolution 1500 instrument (microbalance sensitivity $\pm 0.1 \mu\text{g}$) at temperatures up to 650°C. All analyses were performed under a constant flow of Ar (20 ml/min). Thermogravimetric Analysis (TGA) and Derivative Thermogravimetric Analysis (DTG) curves were prepared under non-isothermal conditions and the decomposition interval of the precursors determined.

The different ZnO samples were also characterised by transmission electron microscopy (TEM) using a JEM2100 HT transmission microscope. In addition, visible photoluminescence (PL) and micro-Raman spectra were obtained using a confocal Horiba Ybon instrument using excitation wavelengths of 325 nm and 633 nm respectively. For the latter two analyses, the ZnO samples were compacted into pellets, by pressing the powders under 1T pressure

3. Results and Discussion

3.1. Characterisation of the black mass and synthesis of the precursors

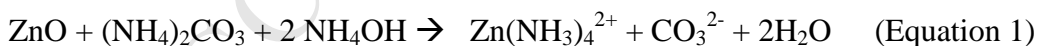
The black mass was mainly composed of Mn (36.8 wt.%) and Zn (23.7 wt.%) with some C (6 wt.%) (Table 1). Around 50% of the Zn was in the form of ZnO and 50% in the form of Zn Mn₂O₄.

The majority crystalline phases of the black mass were ZnO (zincite) and ZnMn₂O₄ (hetaerolite), plus smaller amounts of KCl (silvite) and Ca₆Mn₈ (Fig.1).

Table 2 shows the results of leaching, evaporation and calcination. The greater the NH₃ content of the leaching solution, the more Zn²⁺ the leachate contained (hence a greater content is expected for the solutions with NH₃ concentrations between 0.5 mol/L and 1 mol/L). The post-evaporation mass of precursor (M_c) obtained also increased with increasing NH₃ in the leaching solution, from 20.83 g/L at 0.1 mol/L NH₃ to 26.05 g/L at 1 mol/L (similar variations were obtained per 100 g of black mass [M_m]).

The mass of ZnO obtained after leaching, evaporation and calcination (M_{ZnO}) increased with the concentration of NH₃ in the leaching solution, from 13.08 g/100 g of black mass for 0.1 mol/L NH₃ to 15.10 g/100 g for 1 mol/L NH₃. The recovery of ZnO (R_{ZnO}) ranged from 42.6 wt.% to 47.6 wt.% for the 0.1 and 1 mol/L NH₃ leaching solutions (the leaching solutions solubilise Zn only when in the form of ZnO (Shin et al., 2008)).

Several complexes were formed during leaching depending on the concentrations of Zn²⁺, NH₄⁺ and CO₃²⁻ (Hubbel, 1926; Spink and Stein, 1989; Rodríguez et al., 1999, Wang and Muhammed, 1999). In an (NH₄)₂CO₃ medium, the extraction reaction for the leaching of ZnO follows Equation 1:



Normally, the soluble species of Zn in this leaching medium is Zn(NH₃)₄CO₃ (Meng and Han, 1996, Rodríguez et al., 1999), with a Zn:NH₃ ratio of 1:4. However, other species of Zn(NH₃)₄CO₃ could appear with a Zn:NH₃ ratio of 1:1 to 1:6 depending on the NH₃ concentration of the solution (Harvey, 2006 and Shin et al., 2008). However, when the Zn or NH₃ concentrations are lower, the basic carbonate Zn₅(OH)₆(CO₃)₂ appears (Table 2) (Buzatu et al., 2013, Moghadman et al., 2014).

3.2. Structural analyses

3.2.1. Precursors

Figure 2 shows the XRD spectra of the different precursors produced. When leaching was performed with the 0.1 mol/L NH_3 (NH_4) $_2\text{CO}_3$ solution, the XRD peaks show that the precursor obtained was the basic carbonate $\text{Zn}_5(\text{CO}_3)_2(\text{OH})_6$ (JCPDS card No. 00-019-1458) and $\text{K}_2\text{CO}_3 \cdot 1.5\text{H}_2\text{O}$ (00-011-0655) see Fig. 2a, while for concentrations of 0.5 and 1 mol/L NH_3 it was $\text{Zn}(\text{NH}_3)(\text{CO}_3)$ (JCPDS card No. 01-088-2016) (Fig. 2b and 2c).

Figure 3 shows the TGA and DTG curves obtained for each precursor. Figure 3a shows those for the decomposition of the basic carbonate $\text{Zn}_5(\text{CO}_3)_2(\text{OH})_6$ under non-isothermal conditions. Decomposition is seen to occur in two stages. In the first, which occurs between 60° C and 138° C, a mass loss of some 1.6 wt.% was caused by the release of hydration water. This is followed by the rapid decomposition of the $\text{Zn}_5(\text{CO}_3)_2(\text{OH})_6$. The DTG curve indicates this to occur between 251 and 308° C, with a peak at 284° C. The TGA curve shows the loss of mass to be 26.1 wt.%, which corresponds to the theoretical value of 25.9 wt.% for this basic carbonate. Between 450° C and 650° C, the TGA curve reveals constant mass loss, suggesting that the decomposition of the $\text{Zn}_5(\text{CO}_3)_2(\text{OH})_6$ leads directly to the formation of ZnO, without passing through intermediate products (e.g., ZnCO_3) (Kanari et al., 2004; Li et al., 2005; Alhami et al., 2015). This decomposition reaction is represented thus:



In the present work, the temperature recorded for this decomposition was higher than reported by other authors for basic carbonates produced via other synthetic routes. For example, the decomposition temperature for a basic carbonate prepared from $\text{Zn}(\text{NO}_3)_2 \cdot 6\text{H}_2\text{O}$ and urea was reported to be 220° C (Liu et al. 2004); 244° C (Li et al., 2005); 244° C (Ariyanto et al., 2009) and finally 180-350° C (Alhawi et al., 2015); for a carbonate produced by the dissolution of analytical grade ZnO in ammoniacal (NH_4) $_2\text{CO}_3$ was reported as 270° C (Moghaddam et al., 2014); for a carbonate obtained by hydrothermal synthesis from hexamethylenetetramine and zinc acetate ($\text{Zn}(\text{O}_2\text{CCH}_3)_2$)

in an NaF medium was 210-450° C (Han et al., 2016); for a carbonate produced by reacting $\text{Zn}(\text{NO}_3)_2$ and $(\text{NH}_4)_2\text{CO}_3$ in ethanol was 220° C (Raoufi, 2013a and Raoufi, 2013b); for a basic carbonate prepared from a simple urea aqueous solution route for the synthesis of zinc hydroxide carbonate and ZnO microcrystals using zinc nitrate as the starting salt was 290° C (Bitenc et al., 2008); for a hydrothermal treatment of zinc nitrate aqueous solution containing urea up to 160° C was 260° C (Music et al., 2002); for a basic carbonate prepared from zinc oxide and ammonium hydrogencarbonated in aqueous solution was 250° C (Dobrydnev et al., 2014) and finally, for hydrothermal treatment of zinc acetate dehydrate and urea at 120° C was 250° C (Hu et al., 2010).

The high decomposition temperature of the present black mass-obtained $\text{Zn}_5(\text{CO}_3)_2(\text{OH})_6$ might be a consequence of impurities in the leachate, especially Cu. Cu can partially replace Zn, giving rise to compounds of the type $(\text{Zn}_x\text{M}_{1-x})_5(\text{CO}_3)_2(\text{OH})_6$, where M = Cu or Co, etc. (Han et al., 2016).

Figures 3b and 3c show the TGA and DTG curves for the $\text{Zn}(\text{NH}_3)(\text{CO}_3)$ obtained with the 0.5 and 1 mol/L NH_3 leaching solutions respectively. The DTG curve in Figure 3b shows the $\text{Zn}(\text{NH}_3)(\text{CO}_3)$ to decompose in two stages. The first, from 110.6 to 184°C, involves the elimination of the water adsorbed onto the surface of the carbonate. In the second, an intense endothermic effect occurs between 248 and 319° C, with a peak at 289° C. The TGA curve shows a mass loss of some 40.2 wt.%, comparable to the theoretical mass loss for this precursor (42.8 wt.%). It also reveals a constant mass loss over the interval 450-650° C, suggesting the reaction proceeds as follows (3):



The DTG curve in Figure 3c (produced with 1 mol/L NH_3 in the leaching solution) shows that the decomposition of the carbonate occurs in a single stage at a temperature of 247-319° C, with a peak at 289° C. The TGA curve shows a mass loss of 41 wt.%, comparable to the theoretical mass loss for this precursor (42.8 wt.%). It also shows a constant mass loss between 450 and 650° C, suggesting the reaction proceeds as in Equation 3.

In the present work, the temperature recorded for the decomposition of the $\text{Zn}(\text{NH}_3)(\text{CO}_3)$ (289°C) was similar than reported by other authors. For example, the decomposition temperature for a zinc ammonium carbonate was reported to be 280°C (Ehret and Greenstone, 1943; Zelanák et al., 2000; Wen et al., 2004)

Figure 4 shows the FTIR spectra for the different precursors. Figure 4a shows the FTIR spectrum for the basic carbonate $\text{Zn}_5(\text{CO}_3)_2(\text{OH})_6$. The bands 1506 and 1387 cm^{-1} (ν_3 frequency) and 1046 , 836 and 707 cm^{-1} (ν_1 frequency) confirm the presence of carbonate groups (Bitenc et al., 2008). The separation of the bands 1506 and 1387 cm^{-1} indicates a high degree of crystallinity (Music et al., 2002). The absorption peak at 3340 cm^{-1} is the stretching vibration of hydrogen bonds, indicating the plentiful existence of hydroxyl groups and the formation of $\text{Zn}_5(\text{CO}_3)_2(\text{OH})_6$.

Figures 4b and 4c show the FTIR spectra for the $\text{Zn}(\text{NH}_3)(\text{CO}_3)$ precursors obtained with 0.5 and 1 mol/L NH_3 in the leaching solution: the curves for both are the same. The presence of the band at 1564 cm^{-1} and the shoulder at 1389 (ν_3 frequency), along with the bands at 845 and 743 cm^{-1} (ν_4 frequency), confirm the presence of carbonate groups. The absorption peaks at 3351 and 3263 cm^{-1} represent the stretching vibration of N-H bonds, indicating the plentiful existence of ammonium groups. In addition, the bands at 1621 and 1243 cm^{-1} (δ_{as}) confirm the presence of N-H bonds.

Figure 5a shows the micro- and nanostructures of the $\text{Zn}_5(\text{CO}_3)_2(\text{OH})_6$ that appeared during the synthesis process. Figures 5b and 5c show those corresponding to the two samples of $\text{Zn}(\text{NH}_3)(\text{CO}_3)$. The $\text{Zn}_5(\text{CO}_3)_2(\text{OH})_6$ shows structures such as microflowers, while the two $\text{Zn}(\text{NH}_3)(\text{CO}_3)$ samples show microrods. In Figure 5c (in which the $\text{Zn}(\text{NH}_3)(\text{CO}_3)$ was produced with 1 mol/L NH_3 in the leaching solution), these rods are apparently surrounded by an amorphous material. This might be excess Zn or impurities such as K_2O ; certainly potassium is present in the starting black mass since it is a component of battery electrolytes.

3.2.2. Characterisation of the ZnO produced from the different precursors

Table 3 shows the chemical composition of the ZnO obtained from the different precursors.

Figure 6 shows TEM images of the ZnO nanoparticles produced from the different precursors, and their respective selected area electron diffraction (SAED) patterns. In all cases the nanoparticles were single-crystal nanometric hexagonal plates; only slight differences between the ZnO samples were seen in terms of hexagonal regularity and edge length. The SAED patterns revealed the values $d_{L1}=2.86 \text{ \AA}$, $d_{L3}=2.82 \text{ \AA}$ and $d_{L2}=2.80 \text{ \AA}$ (where L1, L2 and L3 refer to the increasing concentration of NH_3 in the leaching solution [0.1 mol/L, 0.5 and 1.0 mol/L NH_3]), which correspond to a lattice spacing of $\{1010\}$ planes. The zone axis in all these planar structures appears parallel to the $[0001]$ direction. The c parameter values were calculated from the SAED patterns as $c_{L1}=5.19 \text{ \AA}$, $c_{L2}=5.21 \text{ \AA}$ and $c_{L3}=5.18 \text{ \AA}$.

Structural characterization of the ZnO samples was completed by XRD and Raman spectroscopy. Figure 7 shows the XRD patterns for each sample; the peaks are indexed as belonging to the wurtzite ZnO phase (JCPDS card No. 01-079-0206). No differences were seen between the different ZnO samples in terms of peak location, shape or amplitude. The definition of the diffraction peaks indicates a high degree of crystallinity. Micro-Raman analysis (Fig. 8) confirmed the presence of wurtzite-phase ZnO (Xu et al., 2004) with Raman optical modes centred at 100 cm^{-1} (E_2), 208 cm^{-1} and 334 cm^{-1} (second order vibrations), 380 cm^{-1} ($A_1 \text{ TO}$), 437 cm^{-1} (E_2) and 583 cm^{-1} ($E_1\text{LO}$). The L3 ZnO sample (i.e., that produced with the 1 mol/L NH_3 leaching solution) showed well defined peaks but also a strong background of red luminescence caused by the use of the 633 nm laser excitation source.

The luminescent properties of compounds are strongly related to their electronic and crystalline structures; the luminescent mechanisms of compounds are therefore strongly influenced by the way in which they are prepared. ZnO luminescence is the result of many different processes, and those at work in the present samples might vary considerably from those taking place in commercial ZnO powders. Intrinsic defects in a ZnO lattice, such as oxygen or zinc vacancies or interstitials, may affect its luminescence (Rodnyi and Khodyuk, 2011, Zeng et al., 2010).

The PL spectra in Figure 9 show two main components for all samples of ZnO. The first component is a high energy emission band (UV-blue band), centred at 412 nm (2.9

eV) in the L1 and L3 ZnO samples, and at 382 nm in the L2 ZnO sample. In samples L1 and L3, this UV-blue band is composed of four weak contributions at 375 nm (3.3 eV), 382 nm (3.2 eV), 412 nm (2.9 eV, the strongest contribution) and 430 nm (2.8 eV). This fourth contribution might be assigned to the presence of oxygen vacancies (Zhu et al., 2008) and has previously been reported as the consequence of either an oxygen deficiency or the presence of non-stoichiometric ZnO_x crystals mainly concentrated at the grain boundaries (Jin et al., 2000) (which might be of interest for producing ZnO for use in gas sensing applications). The 412 nm contribution might correspond to radiative transitions from neutral or charged Zn interstitial levels to valence or near-valence band acceptor energy states (Rodnyi and Khodyuk, 2011). However this adscription is not clear and several authors, for instance Fan et al., 2005, attribute it to transitions from Zn vacancy energy levels to shallow acceptor energy states.

The UV-blue band of sample L2 is composed of two contributions centred at 375 nm (3.3 eV) and 382 nm (3.2 eV). The first of these either corresponds to band gap emission or to radiative processes linked to longitudinal optic phonons (Xu et al., 2004). The second, a near band edge transition, is proposed by some authors to be due to mechanisms of recombination of free excitons via exciton-exciton collisions (Jin et al., 2000, Zhu et al., 2008, Ghosh et al., 2011). The lack of the 430 nm (2.8 eV) contribution seen in the L1 and L3 samples might indicate that the x parameter (describing the stoichiometry of the ZnO_x crystal) has a value close to one or slightly higher, which would points toward a certain Zn deficiency. Since all the precursors were calcined under similar oxidising atmospheres, the cause of the PL variations between the samples in the UV-blue band can only be the result of the different NH_3 concentrations of the leaching solution.

The second luminescent component in the spectra is a broad green-yellow band. This dominates the spectrum of all the ZnO samples. The strongest contribution to this component is centred at 527 nm (2.35 eV). The origin of this band is uncertain, although it is known to be composed of multiple contributions. This band mainly reflects transitions involving intrinsic defects such as Zn interstitials, oxygen vacancies and Zn vacancies, along with complex extrinsic defects. The literature indicates that the contribution centred at 527 nm (2.35 eV) is characteristic of oxygen-rich samples, with Zn vacancies responsible for its emission (Xu et al., 2004). Calcination in an oxidising

atmosphere is not the only way to increase the concentration of Zn vacancies; alkaline elements such as Li or K could also promote their formation (Zhu et al., 2008) by reducing their formation energy. The greater intensity of the L2 ZnO green-yellow band compared to those of L1/L3 suggests that oxygen vacancies might not play an important role in the luminescence observed, and might indicate it to be largely caused by Zn vacancy-related transitions. The observed Zn deficiency of the L2 sample might have favoured transitions between Zn vacancy levels, leading to the enhancement of the green-yellow band. On the other hand, the slight shoulder observed around 600nm, would reinforce our hypothesis about the role of the alkaline (Urbiet al., 2001).

4. Conclusions

ZnO was obtained from spent batteries by leaching, evaporation and calcination. The NH_3 concentration of the leaching solutions was critical in the type of post-evaporation precursor produced: $\text{Zn}_5(\text{CO}_3)_2(\text{OH})_6$, at 0.1 mol/L, and $\text{Zn}(\text{NH}_3)(\text{CO}_3)$ at 0.5 and 1.0 mol/L. The ZnO produced by the calcination of these precursors showed nanostructures, good crystalline quality, and few impurities. Structural measurements indicated wurtzite phase ZnO to be dominant in the final products obtained from all precursors.

Photoluminescence analysis showed the crystallization process to be strongly dependent on the NH_3 concentration of the leaching solution, which might induce intrinsic defects in the stoichiometry of O and Zn in the ZnO lattice. However, the luminescent bands obtained, and their relative intensities, are comparable to those reported for commercial ZnO powders. The 'tunability' of the PL bands during ZnO synthesis might be possible, allowing the production of ZnO with different specifications for different applications.

Moreover we have demonstrated that ZnO can be recovered from spent batteries by the proposed leaching/thermal decomposition process. The ZnO produced may differ in its PL properties depending on the concentration of NH_3 in the leaching solution, allowing for ZnO of required specifications to be manufactured.

ACKNOWLEDGEMENTS

This work has supported by the Envirobat España S.L. and by the Spanish Ministerio de Economía y Competitividad MINECO (Projects MAT 2012-31959 and CSD2009-00013) and MINECO/FEDER (MAT2015-65274-R; 2016-2019).

Dr. Irene García-Díaz expresses her gratitude to the Ministry of Economy and Competitiveness for their Postdoctoral Junior Grants (Ref. FPD1-2013-16391) contracts co-financed by the European Social Fund.

PhD. Ana López Fernández expresses her gratitude to the Comunidad de Madrid for their Technical Junior Grants (Ref. PEJ15/AMB/AI-0049) contracts co-financed by the European Social Fund.

Figure Captions

Figure 1. XRD pattern of the initial black mass.

Figure 2. XRD patterns of the precursors obtained with the: a) 0.1 mol/L; b) 0.5 mol/L; and c) 1 mol/L ammoniacal ammonium carbonate leaching solutions.

Figure 3. TGA and DTG curves, obtained under non-isothermal conditions, for the different precursors obtained with the: a) 0.1 mol/L; b) 0.5 mol/L; and c) 1 mol/L NH_3 ammoniacal ammonium carbonate leaching solutions.

Figure 4. FTIR spectra of the precursors obtained with the: a) 0.1 mol/L; b) 0.5 mol/L; and c) 1 mol/L ammoniacal ammonium carbonate leaching solutions..

Figure 5. SEM images. a) microflower of $\text{Zn}_5(\text{CO}_3)_2(\text{OH})_6$ (obtained with 0.1 mol/L NH_3 (NH_4) $_2\text{CO}_3$ leaching solution); b) and c) microrods of $\text{Zn}(\text{NH}_3)(\text{CO}_3)$ (obtained with the 0.5 mol/L and 1 mol/L ammoniacal ammonium carbonate leaching solutions).

Figure 6. TEM images of the ZnO obtained with different ammoniacal ammonium carbonate leaching solutions.

Figure 7. XRD patterns for the ZnO obtained with different ammoniacal ammonium carbonate leaching solutions.

Figure 8. Raman spectra of the ZnO samples (incident wavelength 633 nm).

Figure 9. PL spectra of the ZnO samples.

Table Captions

Table 1. Chemical composition of the starting black mass.

Table 2. Result of leaching, evaporation and calcination.

Table 3. Chemical composition of the ZnO obtained from the different precursors.

References

- Ahn, C.H., Kim, Y.Y., Kim, D.C., Mohanta, S.K., Cho, H.K., 2009. A comparative analysis of deep level emission in ZnO layers deposited by various methods. *J. Appl. Phys.* 105, 13502. <http://dx.doi.org/10.1063/1.3054175>
- Alhawi, T., Rehan, M., York, D., Lai, X., 2015. Synthesis of Zinc Carbonate Hydroxide Nanoparticles Using Microemulsion Process. *Procedia Eng.* 102, 346–355. <http://dx.doi.org/10.1016/j.proeng.2015.01.158>
- Alhawi, T., Rehan, M., York, D., Lai, X., 2015. Hydrothermal Synthesis of Zinc Carbonate Hydroxide Nanoparticles. *Procedia Eng.* 102, 356–361. <http://dx.doi.org/10.1016/j.proeng.2015.01.161>
- Ariyanto, N.P., Abdullah, H., Shaari, S., Junaidi, S., Yulianto, B., 2009. Preparation and Characterisation of Porous Nanosheets Zinc Oxide Films: Based on Chemical Bath Deposition. *World. Appl. Sci. J.* 6, 764–768.
- Audebrand, N., Auffrédic, J.-P., Louër, D., 1998. X-ray Diffraction Study of the Early Stages of the Growth of Nanoscale Zinc Oxide Crystallites Obtained from Thermal Decomposition of Four Precursors. General Concepts on Precursor-Dependent Microstructural Properties. *Chem. Mater.* 10, 2450–2461. <http://dx.doi.org/10.1021/cm980132f>
- Baskoutas, S., Giabouranis, P., Yannopoulos, S.N., Dracopoulos, V., Toth, L., Chrissanthopoulos, A., Bouropoulos, N., 2007. Preparation of ZnO nanoparticles by thermal decomposition of zinc alginate. *Thin Solid Films.* <http://dx.doi.org/10.1016/j.tsf.2007.03.150>
- Bitenc, M., Marinšek, M., Crnjak Orel, Z., 2008. Preparation and characterization of zinc hydroxide carbonate and porous zinc oxide particles. *J. Eur. Ceram. Soc.* 28, 2915–2921. <http://dx.doi.org/10.1016/j.jeurceramsoc.2008.05.003>
- Buzatu, T., Popescu, G., Birloaga, I., Săceanu, S., 2013. Study concerning the recovery of zinc and manganese from spent batteries by hydrometallurgical processes. *Waste Manag.* 33, 699–705. <http://dx.doi.org/10.1016/j.wasman.2012.10.005>
- Buzatu, T., Popescu, G., Birloaga, I., Săceanu, S., 2013. Study concerning the recovery of zinc and manganese from spent batteries by hydrometallurgical processes. *Waste Manag.* 33, 699–705. <http://dx.doi.org/10.1016/j.wasman.2012.10.005>
- Chou, S.M., Teoh, L.G., Lai, W.H., Su, Y.H., Hon, M.H., 2006. ZnO:Al Thin Film Gas Sensor for Detection of Ethanol Vapor. *Sensors* 6, 1420–1427. <http://dx.doi.org/10.3390/s6101420>
- Deep, A., Kumar, K., Kumar, P., Kumar, P., Sharma, A.L., Gupta, B., Bharadwaj, L.M., 2011. Recovery of Pure ZnO Nanoparticles from Spent Zn-MnO₂ Alkaline

- Batteries. Environ. Sci. Technol. 45, 10551–10556.
<http://dx.doi.org/10.1021/es201744t>
- Djurišić, A.B., Ng, A.M.C., Chen, X.Y., 2010. ZnO nanostructures for optoelectronics: Material properties and device applications. Prog. Quantum Electron. 34, 191–259.
<http://dx.doi.org/10.1016/j.pquantelec.2010.04.001>
- Dobrydnev, S.V., Molodtsova M.Yu, Kizim, N.F., 2014. Synthesis and study of basic zinc carbonate. Russ. J. Inor. Chem., 59 (8), 798–800.
<http://dx.doi.org/10.1134/S0036023614080038>
- Ehret, W., Greenstone, A., 1943. Red zinc oxide. J. Am. Chem. Soc., 65, pp. 872–877
- Fan, X.M., Lian, J.S., Guo, Z.X., Lu, H.J., 2005. Microstructure and photoluminescence properties of ZnO thin films grown by PLD on Si(111) substrates. Appl. Surf. Sci. 239, 176–181. <http://dx.doi.org/10.1016/j.apsusc.2004.05.144>
- Ghosh, S., Khan, G.G., Das, B., Mandal, K., 2011. Vacancy-induced intrinsic d0 ferromagnetism and photoluminescence in potassium doped ZnO nanowires. J. Appl. Phys. 109, 123927. <http://dx.doi.org/10.1063/1.3601340>
- Grym, J., Fernández, P., Piqueras, J., 2005. Growth and spatially resolved luminescence of low dimensional structures in sintered ZnO. Nanotechnology 16, 931–935.
<http://dx.doi.org/10.1088/0957-4484/16/6/051>
- Han, W., Yang, K., Li, D., Zhang, Z., Ma, J., Ni, S., Yang, X., 2016. The fabrication and characterization of $\text{Zn}_5(\text{CO}_3)_2(\text{OH})_6$ as a new anode material for lithium ion batteries. Mater. Lett. 164, 148–151.
<http://dx.doi.org/10.1016/j.matlet.2015.10.102>
- Harvey, T.G., 2006. The hydrometallurgical extraction of zinc by ammonium carbonate: A review of the schanabel process. Miner. Process. Extr. Metall. Rev. 27, 231–279.
<http://dx.doi.org/10.1080/08827500600815271>
- Hu, Shao-Hwa, Chen, Y., Hwang, C., Peng, C., Gong, D., 2010. Analysis of Growth Parameters for Hydrothermal Synthesis of ZnO Nanoparticles through a Statistical Experimental Design Method. J. Mater. Sci. 45(19): 5309–17.
<http://dx.doi.org/10.1007/s10853-010-4576-3>
- Hubbell, A.H., 1926. Leaching zinc-lead ores with gas-house liquor. Eng. Min. J. 122, 855–857.
- Jin, B., Im, S., Lee, S., 2000. Violet and UV luminescence emitted from ZnO thin films grown on sapphire by pulsed laser deposition. Thin Solid Films 366, 107–110. [http://dx.doi.org/10.1016/S0040-6090\(00\)00746-X](http://dx.doi.org/10.1016/S0040-6090(00)00746-X)
- Kanari, N., Mishra, D., Gaballah, I., Dupré, B., 2004. Thermal decomposition of zinc carbonate hydroxide. Thermochim. Acta.
[http://dx.doi.org/10.1016/S0040-6031\(03\)00396-4](http://dx.doi.org/10.1016/S0040-6031(03)00396-4)

- Keis, K., Magnusson, E., Lindström, H., Lindquist, S.-E., Hagfeldt, A., 2002. A 5% efficient photoelectrochemical solar cell based on nanostructured ZnO electrodes. *Sol. Energy Mater. Sol. Cells* 73, 51–58. [http://dx.doi.org/10.1016/S0927-0248\(01\)00110-6](http://dx.doi.org/10.1016/S0927-0248(01)00110-6)
- Khalil, M.I., Al-Qunaibit, M.M., Al-zahem, A.M., Labis, J.P., 2014. Synthesis and characterization of ZnO nanoparticles by thermal decomposition of a curcumin zinc complex. *Arab. J. Chem.* <http://dx.doi.org/10.1016/j.arabjc.2013.10.025>
- Khazeni, N., Foudazi, R., Ghassemi, A., 2016. Zn(NH₃)(CO₃) inorganic helical framework for selective separation of carbon dioxide. *Chem. Eng. J.* 304, 369–375. <http://dx.doi.org/10.1016/j.cej.2016.06.084>
- Kołodziejczak-Radzimska, A., Jesionowski, T., 2014. Zinc Oxide—From Synthesis to Application: A Review. *Materials* 7(4): 2833–81. <http://dx.doi.org/10.3390/ma7042833>
- Li, Z., Shen, X., Feng, X., Wang, P., Wu, Z., 2005. Non-isothermal kinetics studies on the thermal decomposition of zinc hydroxide carbonate. *Thermochim. Acta.* <http://dx.doi.org/10.1016/j.tca.2005.08.026>
- Lima, S.A.M., Sigoli, F.A., Jafelicci M., J., Davolos, M.R., 2001. Luminescent properties and lattice defects correlation on zinc oxide. *Int. J. Inorg. Mater.* [http://dx.doi.org/10.1016/S1466-6049\(01\)00055-1](http://dx.doi.org/10.1016/S1466-6049(01)00055-1)
- Liu, Y., Zhao, J., Zhang, H., Zhu, Y., & Wang, Z., 2004. Thermal decomposition of basic zinc carbonate in nitrogen atmosphere. *Thermochim. Acta*, 414(2), 121–123. <http://doi.org/10.1016/j.tca.2003.12.004>
- Meng, X., Han, K.N., 1996. The Principles and Applications of Ammonia Leaching of Metals—A Review. *Miner. Process. Extr. Metall. Rev.* 16, 23–61. <http://dx.doi.org/10.1080/08827509608914128>
- Moghaddam, J., Ghaffari, S.B., Sarraf-Mamoory, R., Mollaesmail, S., 2014. The Study on the Crystallization Conditions of Zn₅(OH)₆(CO₃)₂ and its Effect on Precipitation of ZnO Nanoparticles from Purified Zinc Ammoniacal Solution. *Synth. React. Inorganic, Met. Nano-Metal Chem.* 44, 895–901. <http://dx.doi.org/10.1080/15533174.2012.740738>
- Musić, S., Popović, S., Maljković, M., Dragčević, Đ., 2002. Influence of synthesis procedure on the formation and properties of zinc oxide. *J. Alloys Compd.* 347, 324–332. [http://dx.doi.org/10.1016/S0925-8388\(02\)00792-2](http://dx.doi.org/10.1016/S0925-8388(02)00792-2)
- Nogueira, C.A., Margarido, F., 2015. Selective process of zinc extraction from spent Zn–MnO₂ batteries by ammonium chloride leaching. *Hydrometallurgy* 157, 13–21. <http://dx.doi.org/10.1016/j.hydromet.2015.07.004>
- Raoufi, D., 2013a. Synthesis and microstructural properties of ZnO nanoparticles prepared by precipitation method. *Renew. Energy* 50, 932–937. <http://dx.doi.org/10.1016/j.renene.2012.08.076>

- Raoufi, D., 2013b. Synthesis and Photoluminescence Characterization of ZnO Nanoparticles. *J. Lumin.* 134: 213–19. <http://dx.doi.org/10.1016/j.jlumin.2012.08.045>
- Rodnyi, P.A., Khodyuk, I. V., 2011. Optical and luminescence properties of zinc oxide (Review). *Opt. Spectrosc.* 111, 776–785. <http://dx.doi.org/10.1134/S0030400X11120216>
- Rodriguez-Torres, I., Valentin, G., Lapique, F., 1999. Electrodeposition of zinc--nickel alloys from ammonia-containing baths. *J. Appl. Electrochem.* 29, 1035–1044. <http://dx.doi.org/10.1023/A:1003610617785>
- Rusu, D.I., Rusu, G.G., Luca, D., 2011. Structural Characteristics and Optical Properties of Thermally Oxidized Zinc Films. *Acta. Phys.Pol. A.* 119, 850-856. <http://dx.doi.org/10.12693/APhysPolA.119.850>
- Salgado, A., 2003. Recovery of zinc and manganese from spent alkaline batteries by liquid–liquid extraction with Cyanex 272. *J. Power Sources* 115, 367–373. [http://dx.doi.org/10.1016/S0378-7753\(03\)00025-9](http://dx.doi.org/10.1016/S0378-7753(03)00025-9)
- Senanayake, G., Shin, S.-M., Senaputra, A., Winn, A., Pugaev, D., Avraamides, J., Sohn, J.-S., Kim, D.-J., 2010. Comparative leaching of spent zinc-manganese-carbon batteries using sulfur dioxide in ammoniacal and sulfuric acid solutions. *Hydrometallurgy* 105, 36–41. <http://dx.doi.org/10.1016/j.hydromet.2010.07.004>
- Señorís, S., Sotillo, B., Urbiet, A., Fernández, P., 2016. Optical spectroscopy characterization of Cu doped ZnO nano- and microstructures grown by vapor-solid method. *J. Alloys Compd.* 687, 161–167. <http://dx.doi.org/10.1016/j.jallcom.2016.06.088>
- Serbent H., Reuter G., Schnabel W., Kossel G., 1980. Waelz process of volatilizing zinc and lead from iron oxide-containing materials. US Patent No. 4,238,222 A.
- Shamsipur, M., Pourmortazavi, S.M., Hajimirsadeghi, S.S., Zahedi, M.M., Rahimi-Nasrabadi, M., 2013. Facile synthesis of zinc carbonate and zinc oxide nanoparticles via direct carbonation and thermal decomposition. *Ceram. Int.* 39, 819–827. <http://dx.doi.org/10.1016/j.ceramint.2012.07.003>
- Shin, S.M., Kang, J.G., Yang, D.H., Sohn, J.S., Kim, T.H., 2008. Selective Leaching of Zinc from Spent Zinc-Carbon Battery with Ammoniacal Ammonium Carbonate. *Mater. Trans.* 49, 2124–2128. <http://dx.doi.org/10.2320/matertrans.MRA2008164>
- Spink, D. R., and Stein, J.Y., 1989. Recovery of zinc values from zinc and iron-bearing sulfide materials. US Patent No. 4,889,694 A.
- Tang, Z.K., Wong, G.K.L., Yu, P., Kawasaki, M., Ohtomo, A., Koinuma, H., Segawa, Y., 1998. Room-temperature ultraviolet laser emission from self-assembled ZnO microcrystallite thin films. *Appl. Phys. Lett.* 72, 3270. <http://dx.doi.org/10.1063/1.121620>

- Tsukazaki, A., Ohtomo, A., Onuma, T., Ohtani, M., Makino, T., Sumiya, M., Ohtani, K., Chichibu, S.F., Fuke, S., Segawa, Y., Ohno, H., Koinuma, H., Kawasaki, M., 2004. Repeated temperature modulation epitaxy for p-type doping and light-emitting diode based on ZnO. *Nat. Mater.* 4, 42–46.
<http://dx.doi.org/10.1038/nmat1284>
- Urbiet, A., Fernández, P., Piqueras, J., Hardalov, C., Sekiguchi, T., 2001. Cathodoluminescence microscopy of hydrothermal and flux grown ZnO single crystals. *J. Phys. D. Appl. Phys.* 34, 2945–2949.
<http://dx.doi.org/10.1088/0022-3727/34/19/303>
- Wahab, R., Ansari, S.G., Kim, Y.S., Dar, M.A., Shin, H.-S., 2008. Synthesis and characterization of hydrozincite and its conversion into zinc oxide nanoparticles. *J. Alloys Compd.* 461, 66–71. <http://dx.doi.org/10.1016/j.jallcom.2007.07.029>
- Wang, L., Muhammed, M., 1999. Synthesis of zinc oxide nanoparticles with controlled morphology. *J. Mater. Chem.* 9, 2871–2878. <http://dx.doi.org/10.1039/a907098b>
- Wang, Z.L., 2004. Zinc oxide nanostructures: growth, properties and applications. *J. Phys. Condens. Matter* 16, R829–R858.
<http://dx.doi.org/10.1088/0953-8984/16/25/R01>
- Wen, F., Chen, J., Kim, J.H., Kim, T., Li, W., 2004. Solvothermal Synthesis and Characterization of $\text{Zn}(\text{NH}_3)\text{CO}_3$ Single Crystal. *MRS Proceedings* 817.
<http://dx.doi.org/10.1557/PROC-817-L6.14>
- Xu, C.X., Sun, X.W., Zhang, X.H., Ke, L., Chua, S.J., 2004. Photoluminescent properties of copper-doped zinc oxide nanowires. *Nanotechnology* 15, 856–861.
<http://dx.doi.org/10.1088/0957-4484/15/7/026>
- Xu, L., Li, Z., Cai, Q., Wang, H., Gao, H., Lv, W., Liu, J., 2010. Precursor template synthesis of three-dimensional mesoporous ZnO hierarchical structures and their photocatalytic properties. *CrystEngComm* 12, 2166.
<http://dx.doi.org/10.1039/b924097g>
- Zelenák, V., Györyová, K., Andogová, E., 2000. Thermoanalytical and Spectral Study of zinc(II) Complexes Containing Theophylline. *Thermochim. Acta* 354(1): 81–88.
[http://dx.doi.org/10.1016/S0040-6031\(00\)00462-7](http://dx.doi.org/10.1016/S0040-6031(00)00462-7)
- Zeng, H., Duan, G., Li, Y., Yang, S., Xu, X., Cai, W., 2010. Blue Luminescence of ZnO Nanoparticles Based on Non-Equilibrium Processes: Defect Origins and Emission Controls. *Adv. Funct. Mater.* 20, 561–572.
<http://dx.doi.org/10.1002/adfm.200901884>
- Zhu, H., Iqbal, J., Xu, H., Yu, D., 2008. Raman and photoluminescence properties of highly Cu doped ZnO nanowires fabricated by vapor-liquid-solid process. *J. Chem. Phys.* 129, 124713. <http://dx.doi.org/10.1063/1.2981050>

Web references

European Portable Battery Association (EPBA). 2015. The collection of waste portable batteries in Europe in view of the achievability of the collection targets set by Batteries Directive 2006/66/EC.

<http://www.epbaeurope.net/documents/Reportontheportablebatterycollectionrates-UpdateDec-15-Exerpt.pdf> (accessed 31.01.17).

Official Journal of the European Union, 2013. Directive 2013/56/EU of the European Parliament and of the Council. <http://eur-lex.europa.eu/legal-content/EN/TXT/?uri=celex%3A32013L0056> (accessed 31.01.17)

Table 1. Chemical composition of the starting black mass.

Compound	wt. %
Na ₂ O	7.75
MgO	0.23
Al ₂ O ₃	0.46
SiO ₂	1.69
P ₂ O ₅	0.99
SO ₃	0.64
Cl	1.76
K ₂ O	6.70
CaO	0.36
TiO ₂	0.191
MnO	43.30
Fe ₂ O ₃	1.42
Co ₃ O ₄	0.03
NiO	0.28
CuO	0.08
ZnO	26.88
SrO	0.04
ZrO ₂	0.01
Nb ₂ O ₅	0.01
CdO	0.01
SnO ₂	0.03
BaO	0.13
La ₂ O ₃	0.05
CeO ₂	0.10
PbO	0.04
C _{total}	8.20
S	0.24

Table 2. Result of leaching, evaporation and calcination.

Sample	(NH ₄)(CO ₃) (mol/L)	NH ₃ (mol/L)	Lixiviation	Evaporation	Calcination	Zn Recovery	
			Zn ²⁺ (g/L)	M _c (g/L)	M _m (g/100 g)	M _{ZnO} (g/ 100 g)	wt. %
L1	1.72	0.1	10.94	20.83	19.30	13.08	42.6
L2	1.72	0.5	12.07	25.93	23.39	14.36	45.2
L3	1.72	1.0	12.89	26.05	25.76	15.10	47.6

Table 3. Chemical composition of the ZnO obtained from the different precursors.

Compound	Wt. %		
	ZnO _(L1)	ZnO _(L2)	ZnO _(L3)
Na ₂ O	-	-	-
MgO	-	0.40	0.42
Al ₂ O ₃	0.08	0.09	-
SiO ₂	0.18	0.16	0.12
P ₂ O ₅	1.47	1.48	1.52
Cl	-	0.03	-
K ₂ O	1.49	4.20	4.28
CaO	0.30	0.34	0.32
TiO ₂	0.03	0.03	0.03
MnO	0.01	0.02	0.02
Fe ₂ O ₃	0.13	0.10	0.12
Co ₃ O ₄	-	-	-
NiO	0.06	0.11	0.09
CuO	0.07	0.17	0.09
ZnO	96.20	92.73	92.97

Figure 1

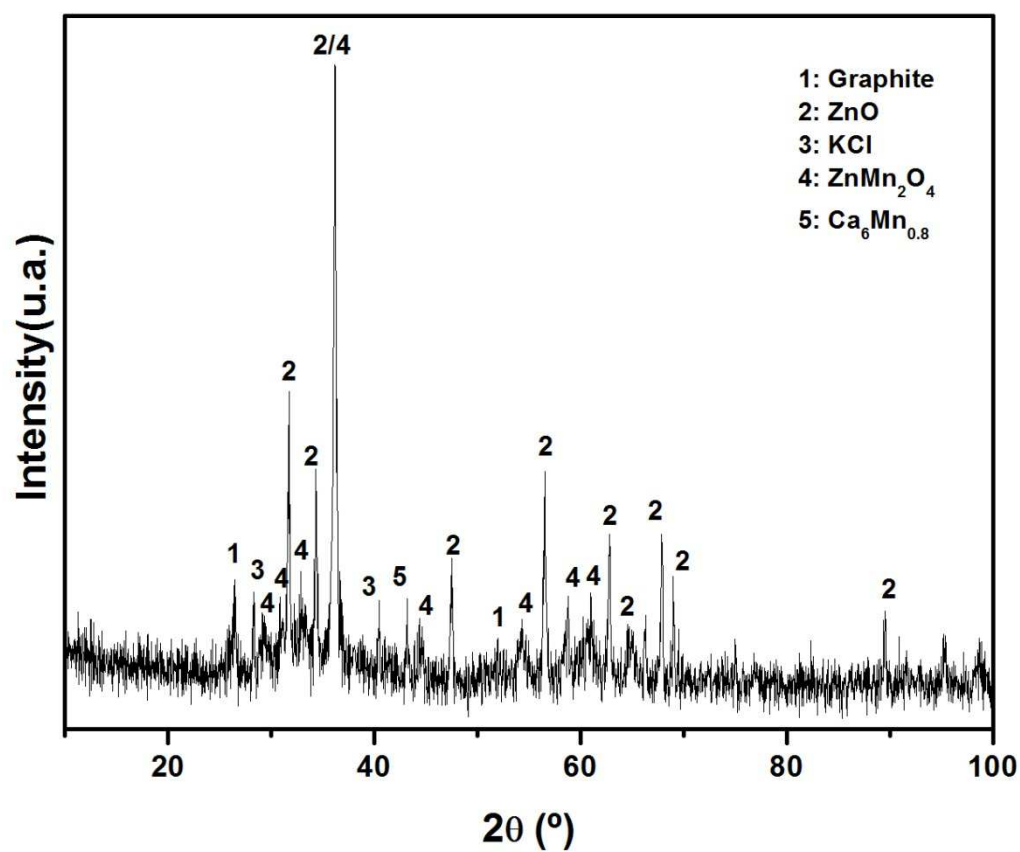
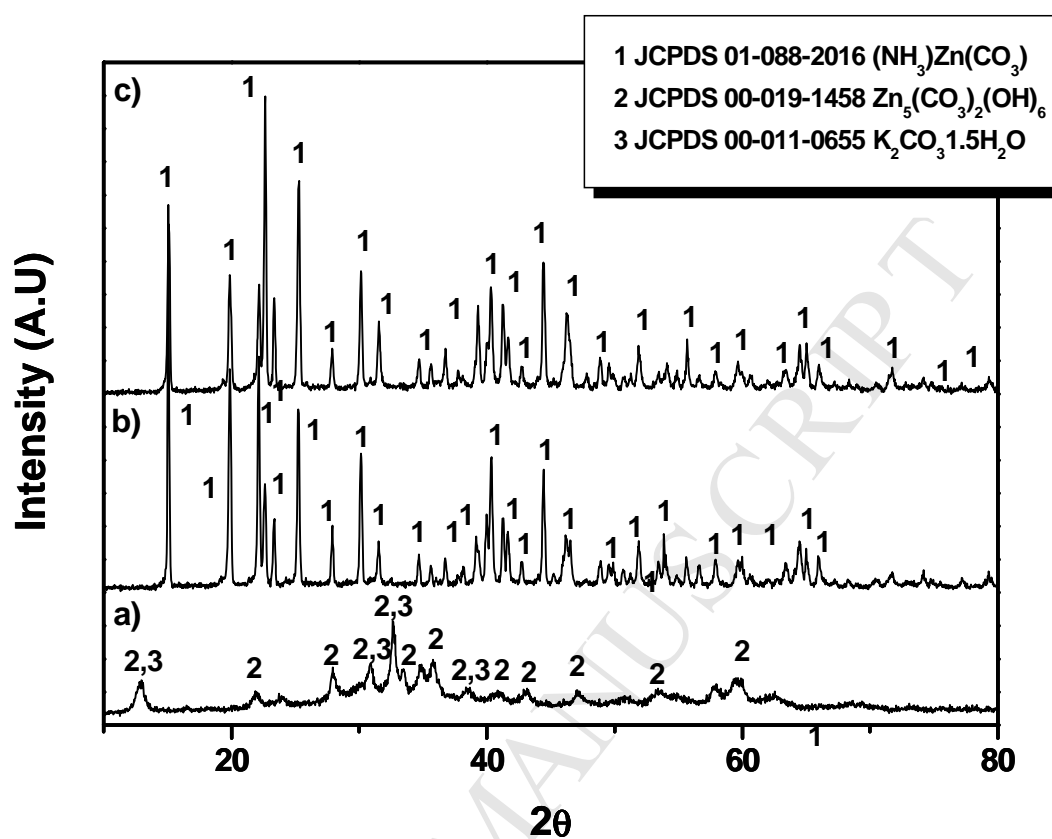
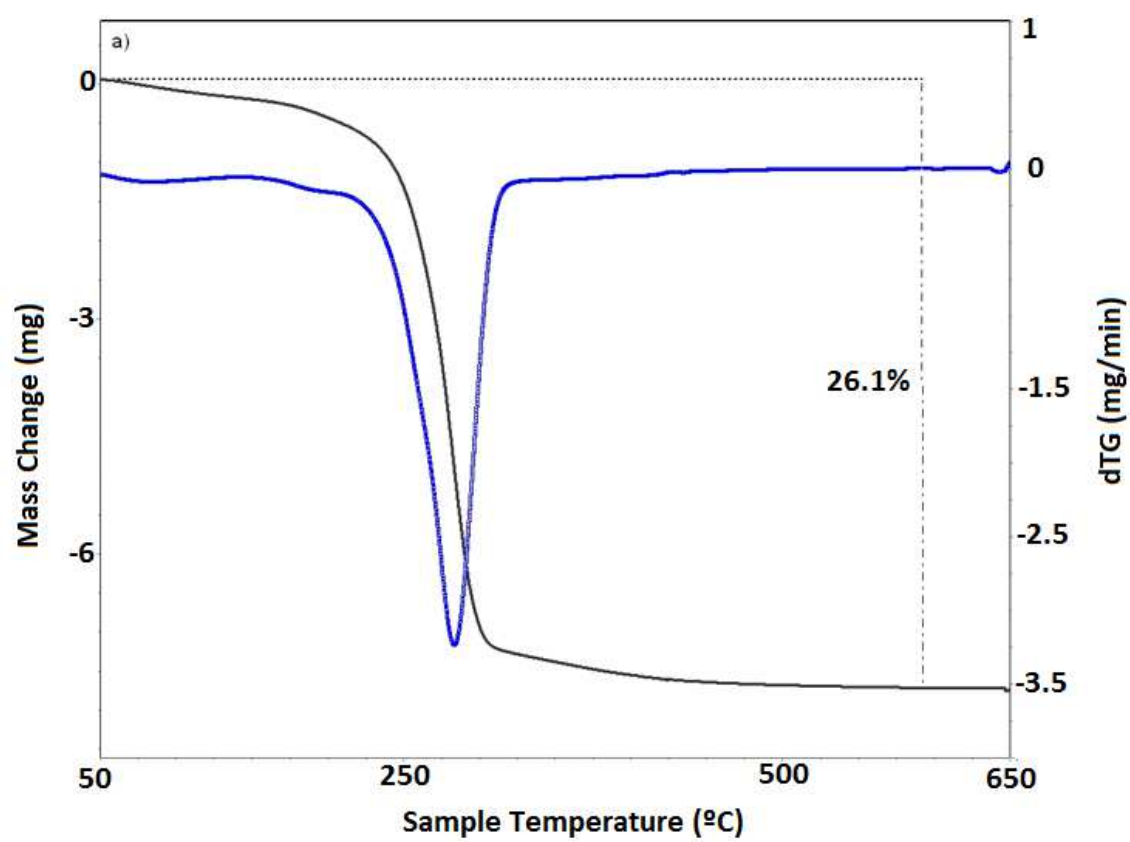
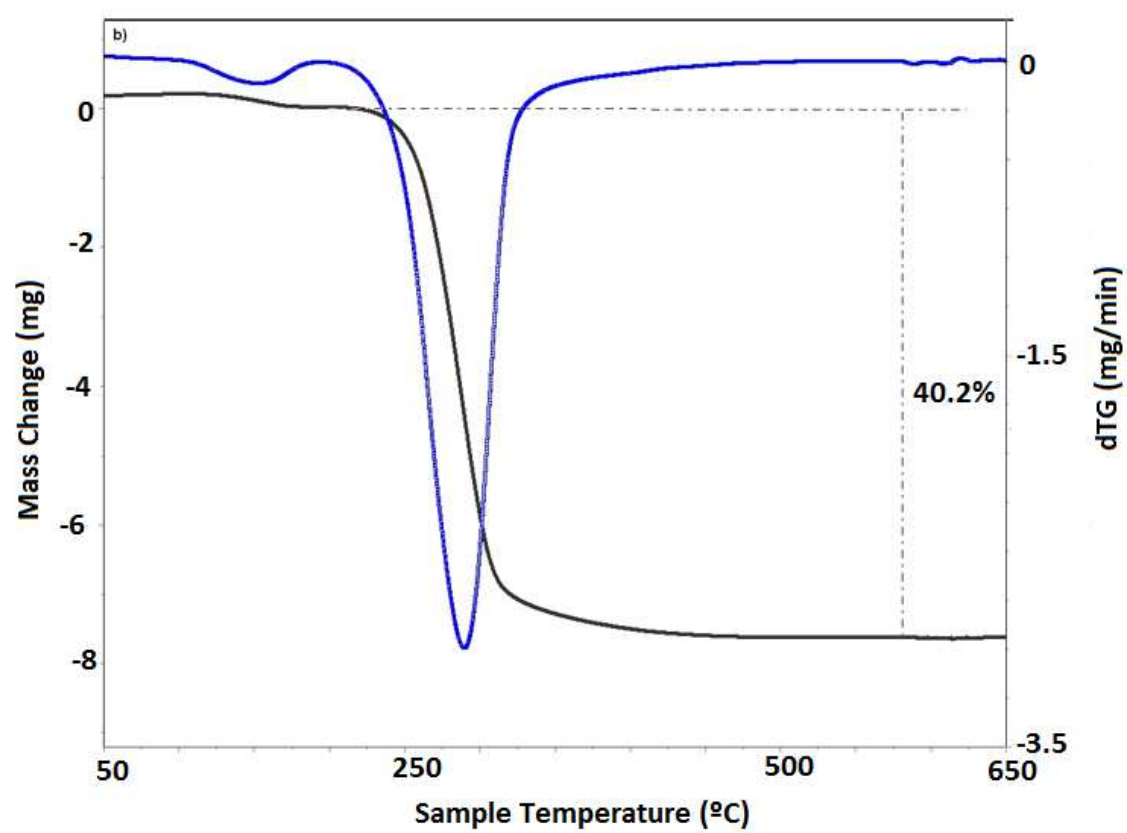


Figure 2







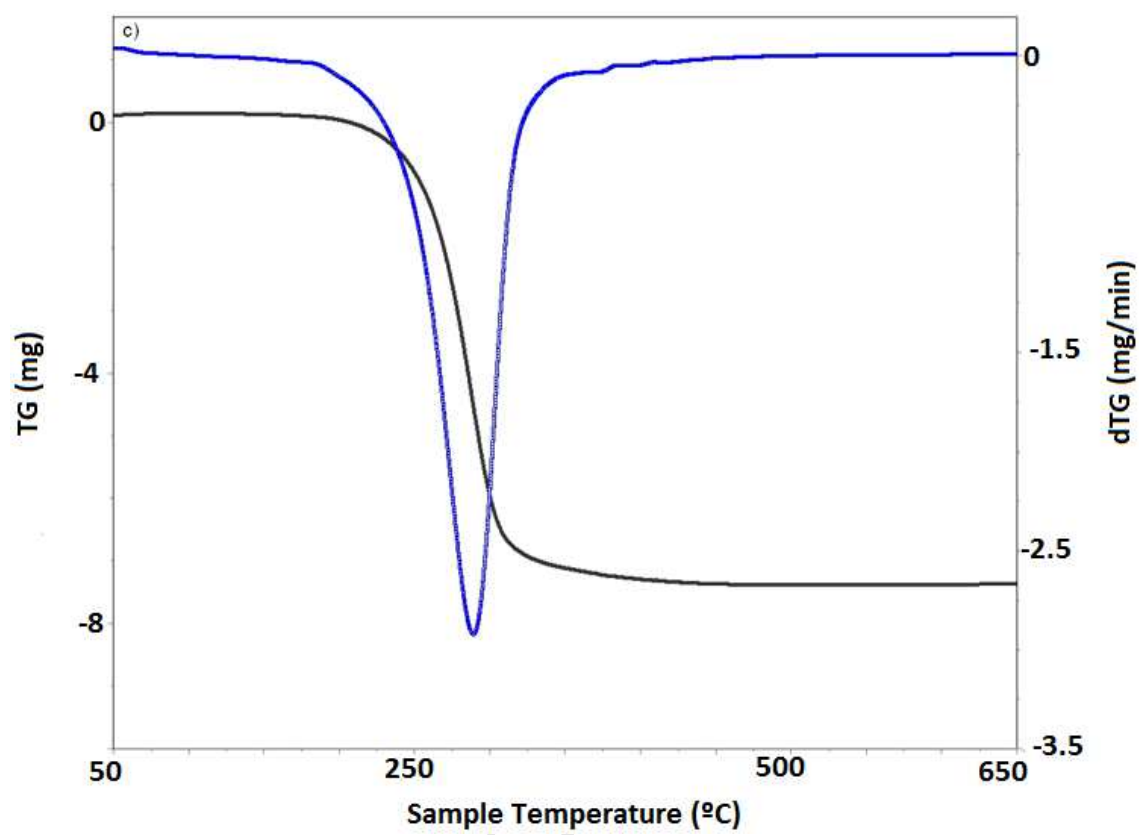
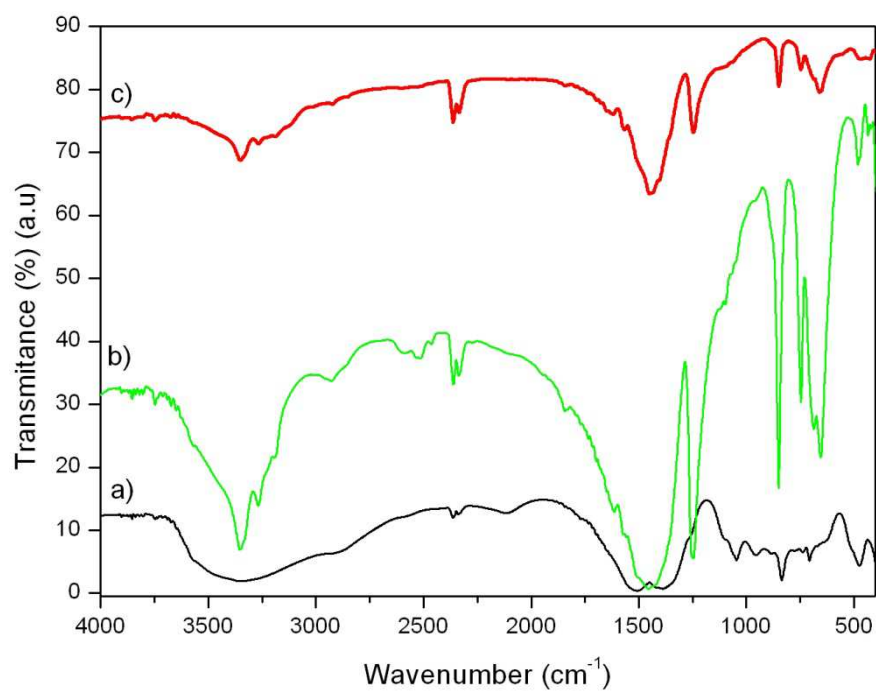
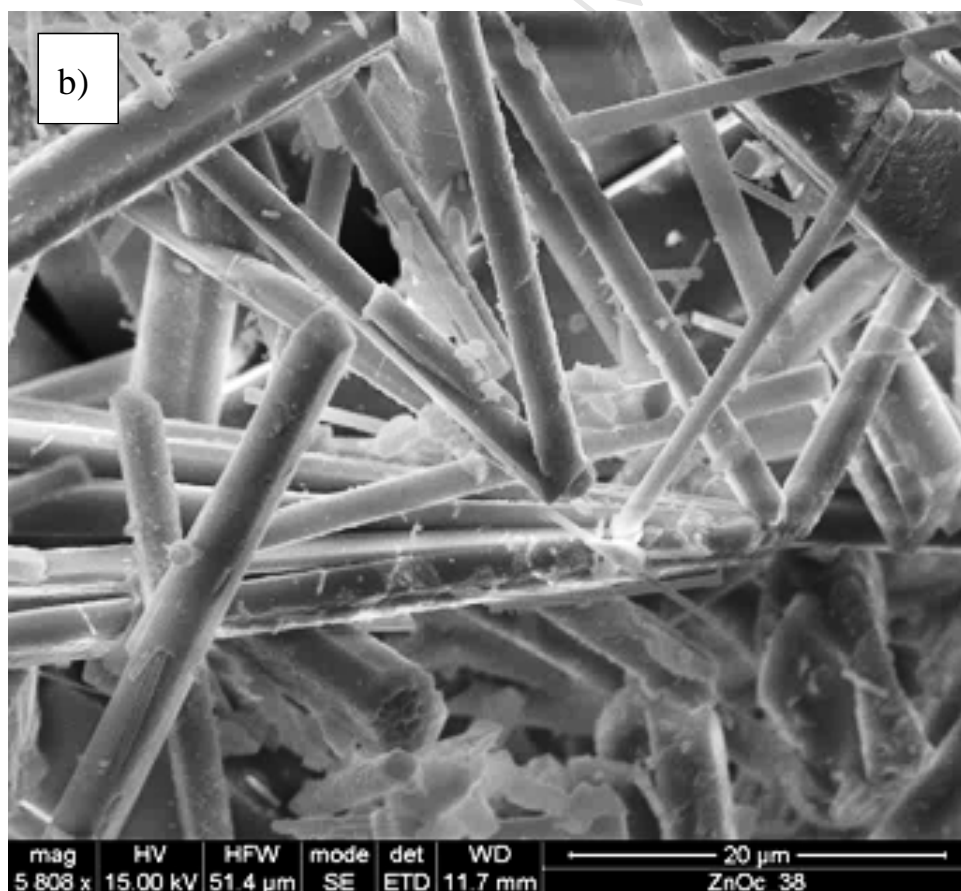
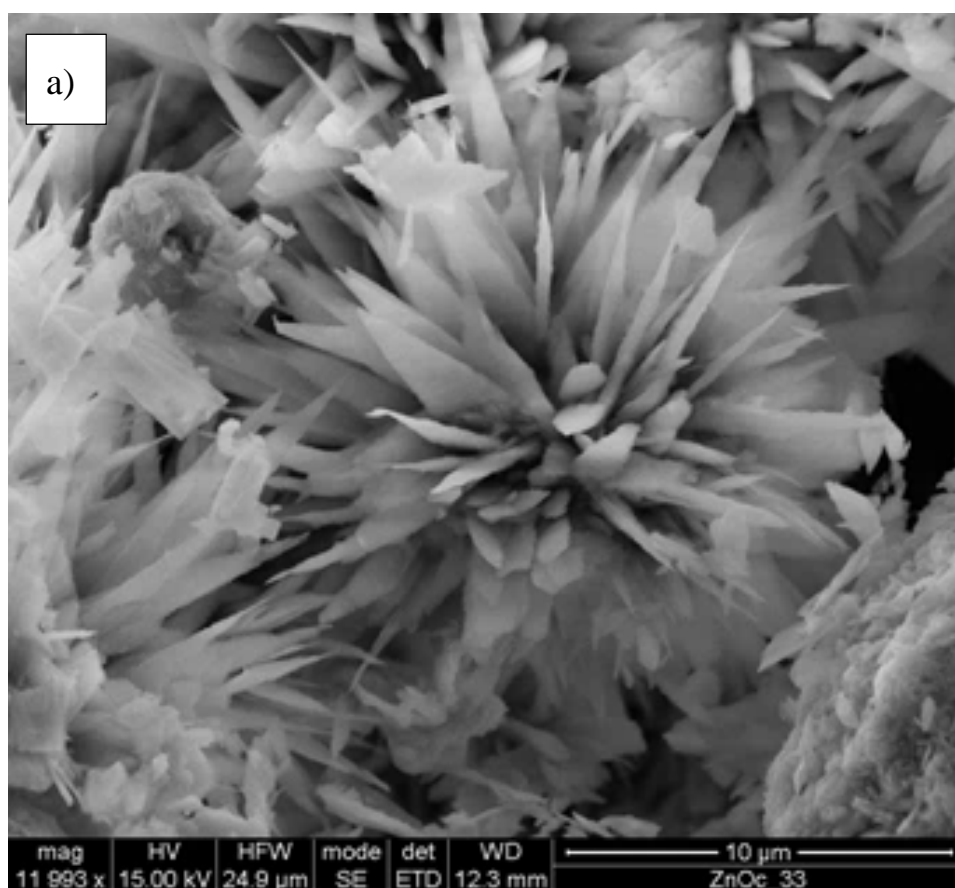


Figure 4





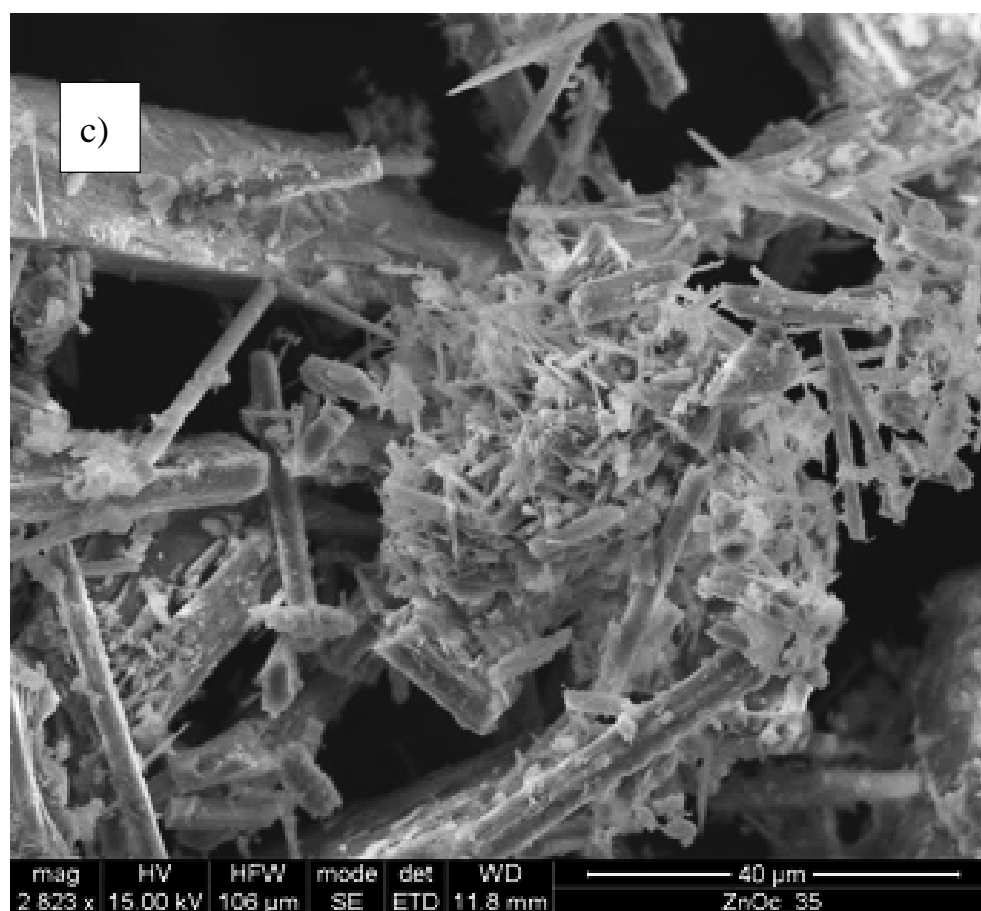


Figure 6

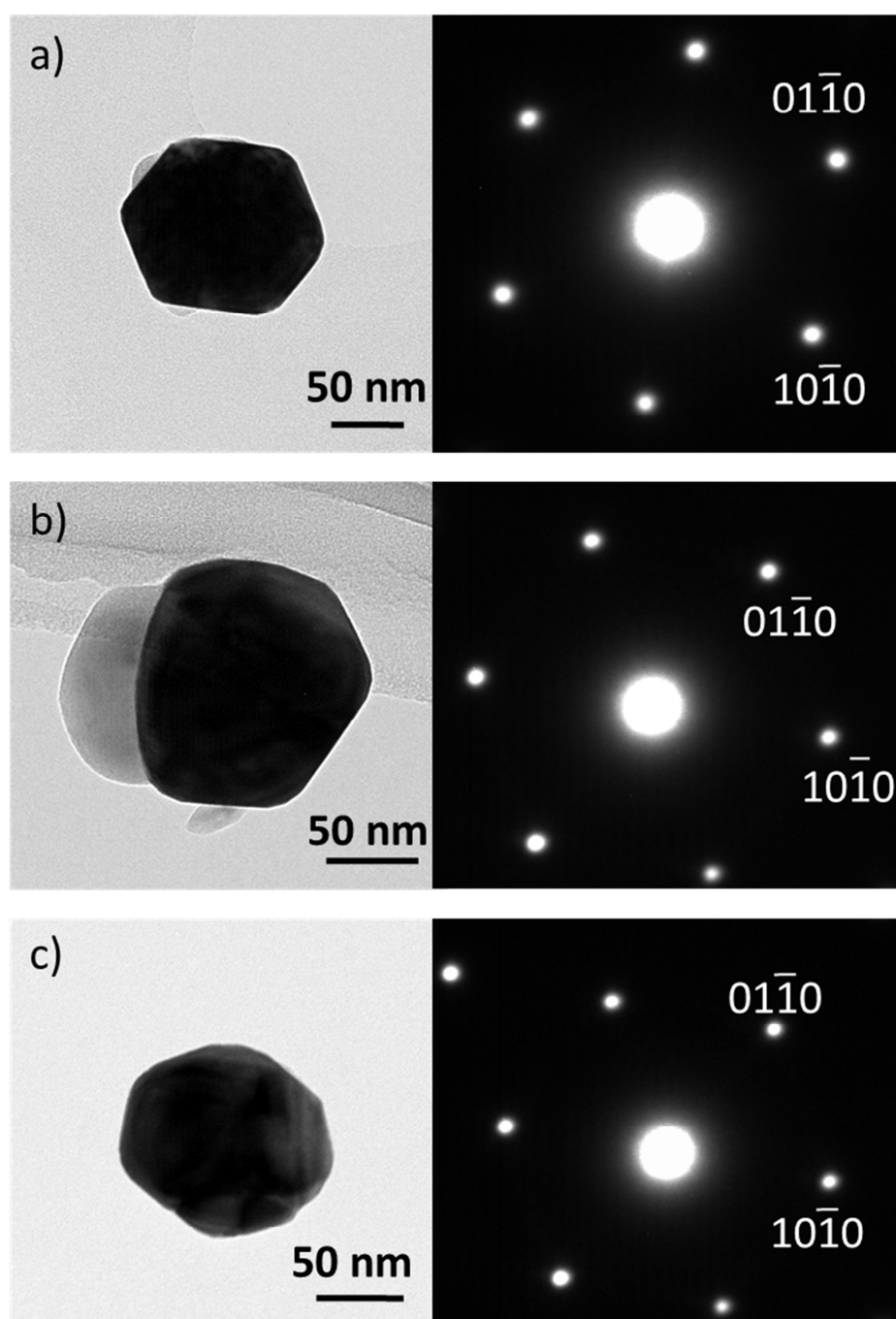


Figure 7

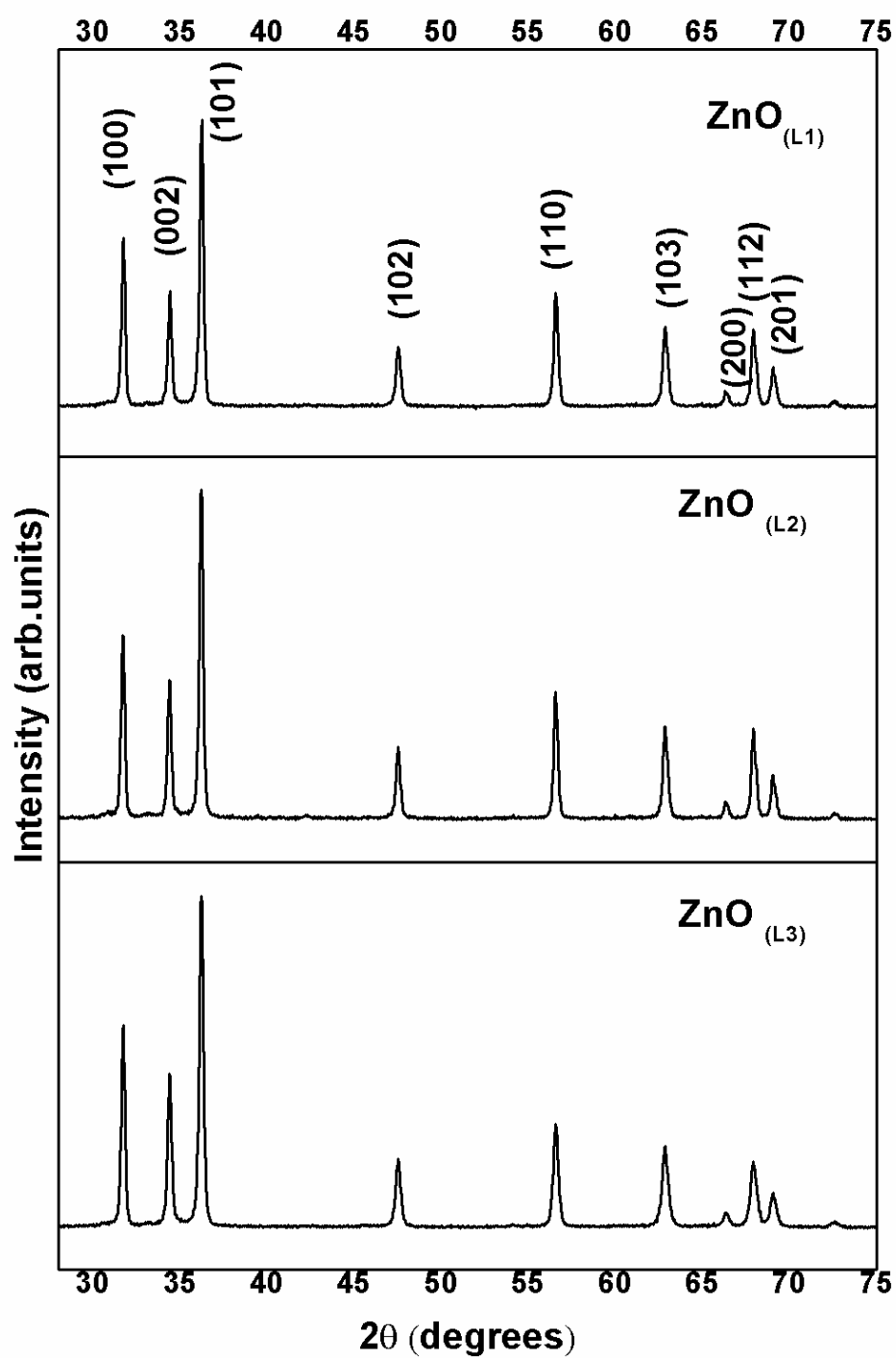


Figure 8

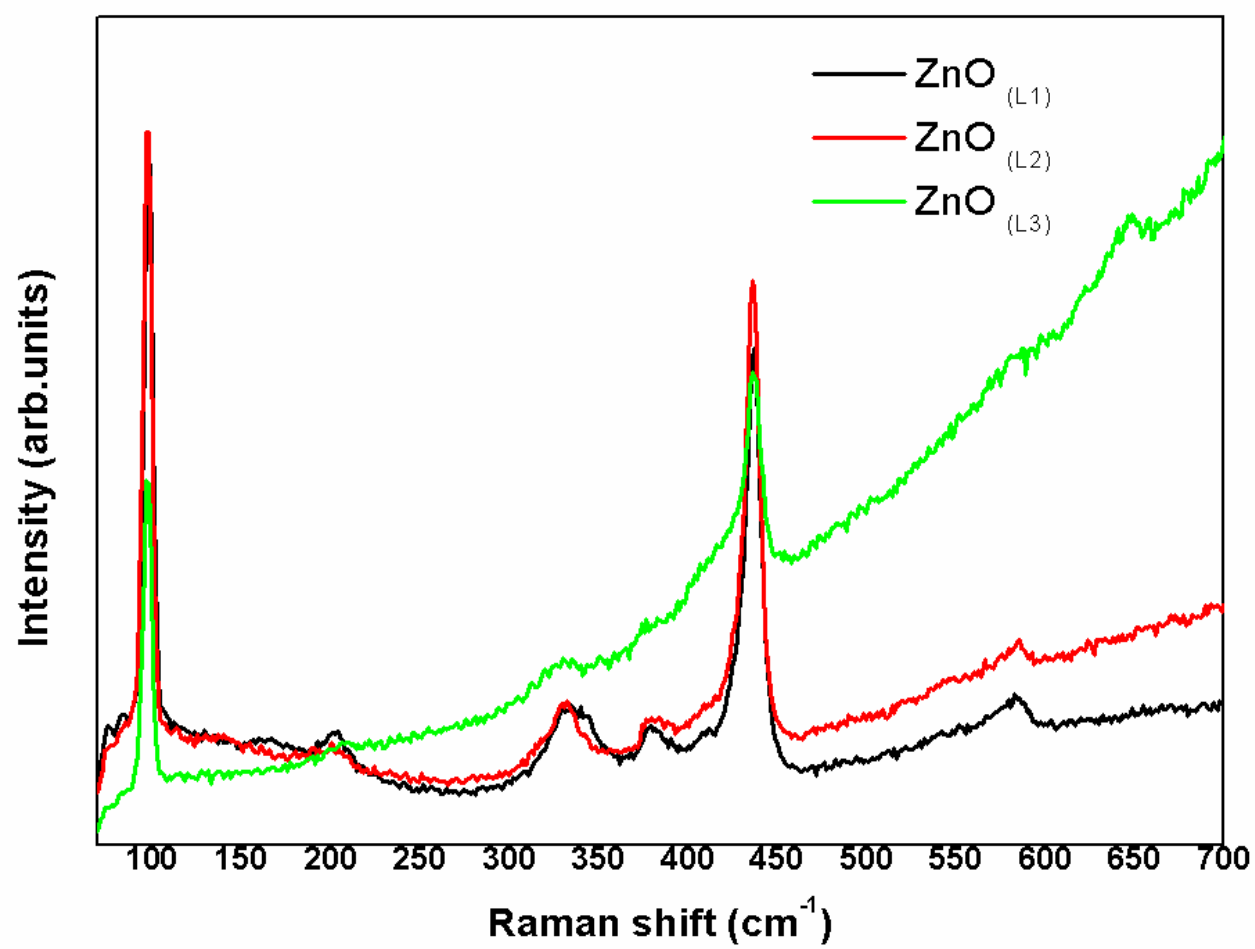
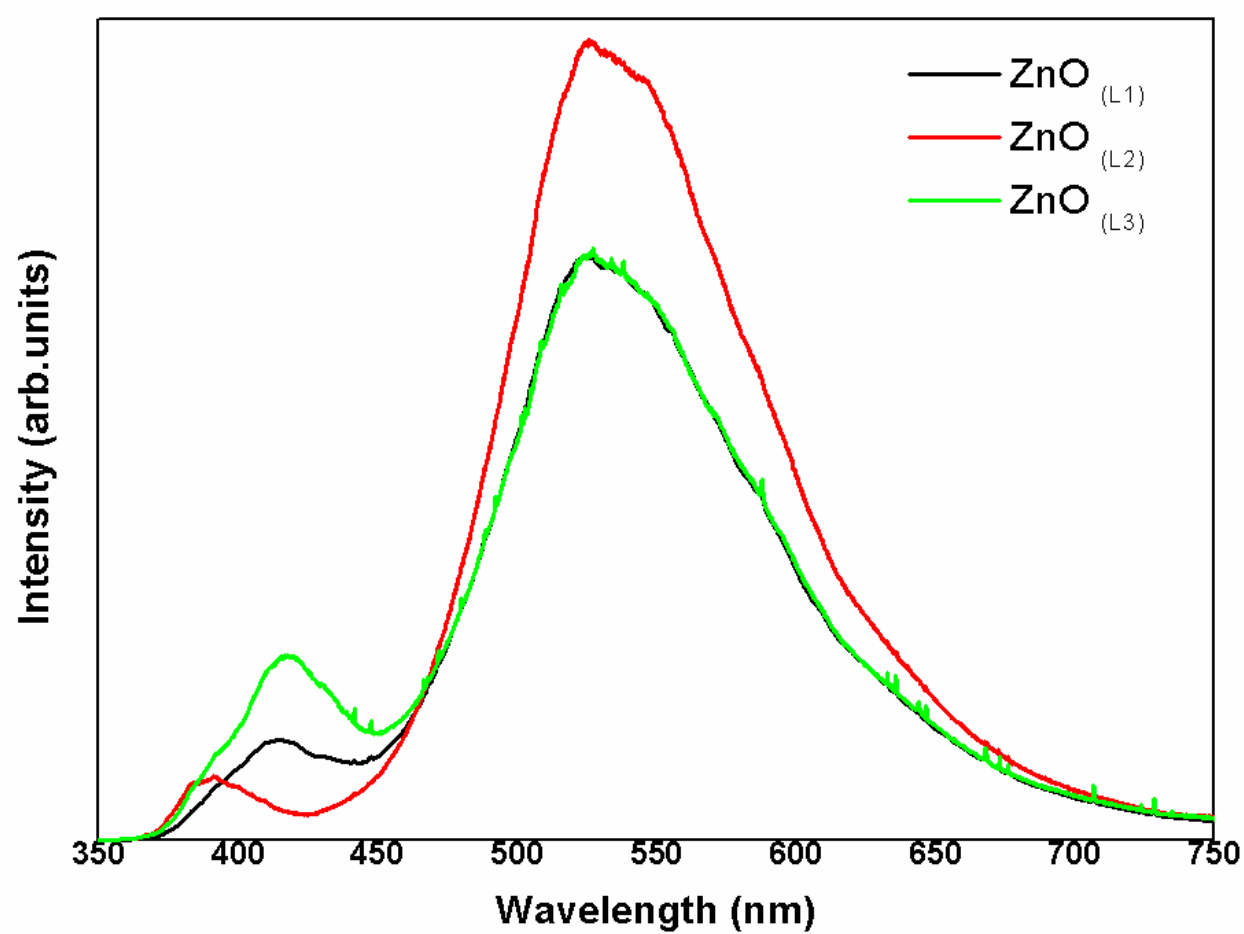


Figure 9



- ZnO obtaining from spent batteries by a leaching, evaporation and calcination
- Wurtzite phase is dominant in the final ZnO obtained
 - ZnO obtained shows nanostructures, good crystalline quality and few impurities
 - “Tunability” of PL bands in ZnO synthesis might allow ZnO for different applications